MIT Open Access Articles

Azulene–Pyridine-Fused Heteroaromatics

1
2
3
4
5
6
7
8
9
10
11
12
13
14
15
16
17
18
19
20
21
22
23
24
25
26
27
28
29
30
31
32
33
34
35
36
37
38
39
40
41
42
43
44
45
46
47
48
49
50
51
52
53
54
55
56
57
58
59
60

Azulene-Pyridine-Fused Heteroaromatics

Hanshen Xin,[†] Jing Li,[‡] Ru-Qiang Lu,[†] Xike Gao,*[‡] and Timothy M. Swager*[†]

[†]Department of Chemistry, Massachusetts Institute of Technology, Cambridge, Massachusetts 02139, United State

[‡]Key Laboratory of Synthetic and Self-Assembly Chemistry for Organic Functional Molecules, Center for Excellence in Molecular Synthesis, Shanghai Institute of Organic Chemistry, Chinese Academy of Sciences, Shanghai 200032, China

ABSTRACT: Azulene, a nonbenzenoid bicyclic aromatic hydrocarbon with unique electronic structure, is a promising building block for constructing nonbenzenoid π-conjugated systems. However, azulene-fused (hetero)aromatics remain rare as a result of limited synthetic methods. We report herein the unexpected synthesis of azulene- and pyridine-fused heteroaromatics **Az-Py-1**, a seven fused ring system with 30π electrons, by reductive cyclization of a 1-nitroazulene. The structure of **Az-Py-1** was unambiguously confirmed by single-crystal X-ray analysis and analogues **Az-Py-2**–**Az-Py-6** were also synthesized, demonstrating that this is an effective method for constructing azulene- and pyridine-fused heteroaromatics. Theoretical calculations, photophysical, and electrochemical studies of **Az-Py-1**–**Az-Py-6** suggest their potential as semiconductors and the single crystal ribbons of **Az-Py-1** show high hole mobilities up to 0.29 cm^2 V^{-1} s^{-1}.

INTRODUCTION

Azulene is a nonbenzenoid 10π electron isomer of naphthalene that has a dipole moment of 1.08 D as a result of electron-rich five-membered ring and an electron-poor seven-membered ring (Figure 1a).[1] These electronic features result in an unoccupied molecular orbital (LUMO) largely localized on the even-positions and a highest occupied molecular orbital (HOMO) with maximum density on the odd-positions (Figure 1b).[2] The segregation of the HOMO and LUMO distinguishes azulene from typical fused benzenoids and also endows azulene with a small HOMO–LUMO energy gap.[2] Azulene exhibits an unusually weak $S_0 \rightarrow S_1$ electronic transition in the visible range, which endows it with its blue color. As a result of these unique electronic and optical properties the synthesis of azulene derivatives for organic materials applications has been an active field of study.[3-18] Noteworthy synthetic processes include regioselective C-H bond activation and coupling at the electron-rich 1-position, which doesn't require directing groups and is not typical for common aromatic hydrocarbons.[19] The low band gaps of azulene derivatives have also attracted increasing attention for applications in organic field-effect transistors (OFET)[20-27] and solar cells.[28-29]

Polycyclic aromatic hydrocarbons (PAHs) are rich with optoelectronic properties and potential applications in organic electronics.[30-32] However, extended PAHs, such as higher acenes, are intrinsically reactive and unstable.[33-35] One of the efficient strategies to overcome this problem is introducing heteroatoms such as N, B, and S into the π-system.[36] These heteroaromatics exhibit enhanced stabilities, as well as impart different chemical and physical properties. On the other hand, recent studies revealed that replacing two benzenoid rings by nonbenzenoid five- and seven-membered rings affords azulene-fused PAHs, with distinctive electronic and structural properties.[37-48] For example, Mastalerz and co-workers reported that PAHs with two embedded azulene moieties display high fluorescence quantum yields in the NIR region.[41] Yasuda and co-workers reported the synthesis of nonalternant hydrocarbons containing two formal azulene units that exhibit antiaromatic character with open-shell singlet biradical features.[43] Recently, Zhang and co-workers reported the synthesis and characterization of a PAH containing two formal azulene units, which violate Kasha's rule with emission from higher excited states and good hole transport properties.[46] However, for most π-conjugated systems containing azulene units, the azulene substructures were generated during later stages of synthesis, and the use of azulene derivatives as starting materials to rationally design and synthesize PAHs and heteroaromatics is limited. Despite the aforementioned advantages, azulene-fused (hetero)aromatics are rare as a result of limited synthetic methods. Herein, we report the synthesis and characterization of a series of azulene- and pyridine-fused heteroaromatics (**Az-Py**s), including 1,10-diheptylazuleno[1,2-*c*]azuleno[2',1':5,6]pyrido[3,4-*g*]isoquinoline (**Az-Py-1**), a seven fused rings system with 30π electrons (Figure 1c). The synthesis of these **Az-Py**s has been developed as a result of an unexpected formal C-H insertion reaction that occurred upon reduction of a 1-nitroazulene precursor with triphenylphosphine. We find that the core apparent C-H process is unique to azulene and is not operative in related 1-nitroaromatic compounds. Most importantly, this reaction provides an effective route to synthesize azulene-pyridine-fused heteroaromatics. The X-ray crystallographic structure of

Az-Py-1, and photophysical and electrochemical properties of these **Az-Py**s are investigated. Moreover, single crystal ribbons of **Az-Py-1** show p-type semiconducting behavior with a high average hole mobility of 0.16 cm^2 V^{-1} s^{-1}.
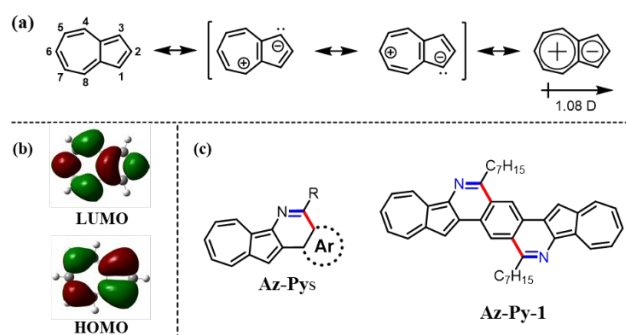
Figure 1. (a) The numbering legend of azulene, its resonance structures and dipole moment. (b) HOMO and LUMO of azulene obtained by DFT calculation. (c) Chemical structures of azulene- and pyridine-fused heteroaromatics in this contribution.

RESULTS AND DISCUSSION

The synthesis of compound **Az-Py-1** is shown in Scheme 1. Reaction of 2-chloroazulene (**1**)[49] with cupric nitrate trihydrate in acetic anhydride gave a 93% yield of 2-chloro-1-nitroazulene (**2**). Suzuki-Miyaura cross-coupling of **2** and 2,2'-(2,5-dioctyl-1,4-phenylene)bis(4,4,5,5-tetramethyl-1,3,2-dioxaborolane) (**3**)[50] afforded 2,2'-(2,5-dioctyl-1,4-phenylene)bis(1-nitroazulene) (**4**) in 81% yield. Our attempt to synthesize **Az-Pyrrole** from **4** using microwave assisted Cadogan cyclization with triphenylphosphine resulted in an unexpected but interesting product, **Az-Py-1**, in 34% yield. The chemical structure of **Az-Py-1** was fully characterized by ^{1}H and ^{13}C NMR spectra. For **Az-Pyrrole**, its carbon spectrum should have 13 sets of peaks in the aromatic region and 8 sets of peaks in the alkyl region. However, ^{13}C NMR spectrum of the product showed 14 sets of peaks in the aromatic region and only 7 sets of peaks in the alkyl region. Notably, a ^{13}C NMR peak at about 157.6 ppm suggests the presence of pyridine structure. MALDI-TOF displays a peak molecular ion [M+H]$^+$ of 577.3616, which is consistent with that of [**Az-Py-1**+H]$^+$ (Calculated [M+H]$^+$: 577.3588), which is also inconsistent [**Az-Pyrrole**+H]$^+$ (Calculated [M+H]$^+$: 581.3901). These results indicate that the product is not the expected **Az-Pyrrole**, but should be **Az-Py-1**.

The pyridine-fused structure of **Az-Py-1** was established with certainty by X-ray single-crystal analysis (Figure 2). Crystals suitable for X-ray diffraction were obtained by slow diffusion of cyclohexane vapor into a solution of **Az-Py-1** in tetrahydrofuran (THF) solution. Compound **Az-Py-1** shows C_{2h}-symmetric character with a relatively planar backbone, as evidenced by the largest dihedral angle of 2.5° among the fused rings. Two C-N bond lengths of **Az-Py-1** are 1.37 Å and 1.31 Å, respectively, which are consistent with the characteristics of aromatic C-N bonds.[51] As depicted in Figure S1, crystal of the **Az-Py-1**

contains two crystallographically independent molecules of **Az-Py-1** in each unit cell (shown in blue and red, respectively). Both two crystallographically independent molecules of **Az-Py-1** adopt one-dimensional sliding π–π stacking pattern and the alternating π-stacked columns arranged in a herringbone-packing motif with a tilt angle of about 139.4° (Figure 2b). The neighboring molecules in each of π-stacked columns exhibit same π–π distance, 3.46 Å, demonstrating a high degree of intermolecular π-π interaction, which is ideal for charge transport within **Az-Py-1** crystals.

Scheme 1. Synthetic route of Az-Py-1.
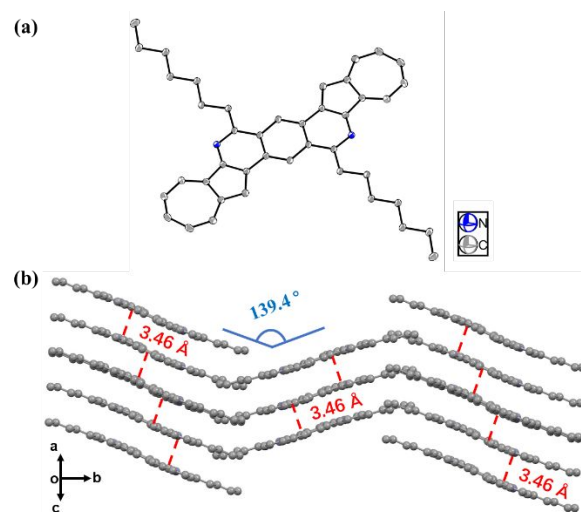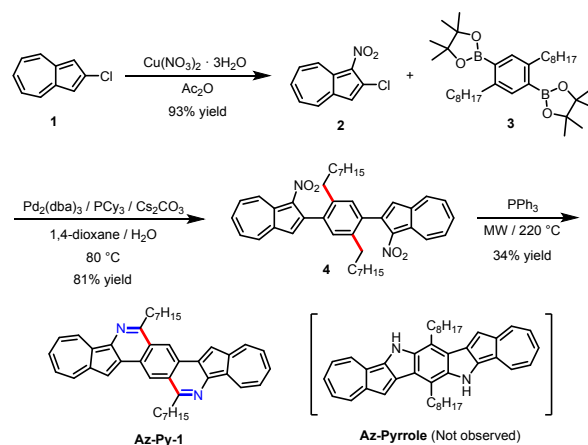
Figure 2. Single crystal structure of **Az-Py-1** (Hydrogen atoms are omitted for clarity): (a) thermal ellipsoids (probability level = 50%); (b) packing structure.

At room temperature, **Az-Py-1**, with two C7 alkyl chains, has a poor solubility in common organic solvents such as dichloromethane, chloroform, THF, and toluene (< 2 mg/mL), which is indicative of strong intermolecular interactions. When heated to 60 °C, its solubility in chloroform and THF is significantly improved (> 5 mg/mL). Thermogravimetric analysis (TGA) and differential scanning calorimetry (DSC) were performed under nitrogen atmosphere to investigate the thermal properties of **Az-Py-1**. TGA measurement demonstrates

that **Az-Py-1** is thermally stable upon the onset decomposition temperatures of 423 °C (Figure S2a). As shown in Figure S2b, in repeated heating–cooling DSC cycles, **Az-Py-1** displays obvious endothermic peak at about 218 °C and exothermic peak at about 172 °C, corresponding to the melting and crystallization processes, respectively.

**Scheme 2. Synthesis of Az-Py-2–Az-Py-6.**
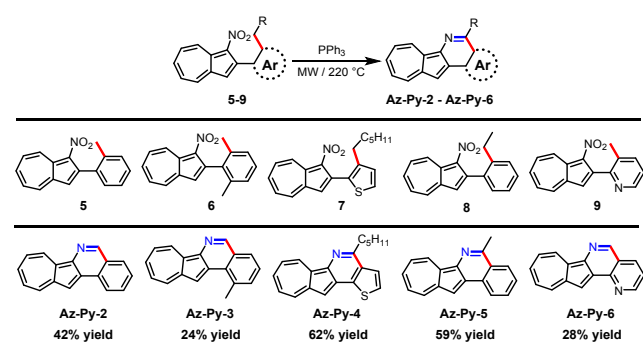
The unexpected generation of **Az-Py-1** and its properties, prompted us to investigate the scope of this cyclization reaction. Compound **5** was synthesized and used as a model substrate to optimize the reaction conditions (Table S1). With the optimized reaction conditions in hand, we evaluated the scope of this reductive cyclization and the results are summarized in Scheme 2. Under the optimized conditions, 1-nitroazulene compounds **5**–**9** provided azulene- and pyridine-fused heteroaromatics **Az-Py-2**–**Az-Py-6** in moderate yields (24%–62%). In accord with our earlier observations, pyrrole-fused products via Cadogan cyclization were not observed. As shown in Scheme 2, substrates with long alkyl chains (**7** and **8**) have higher yields than those requiring reactions with methyl groups (**5**, **6** and **9**). It has been reported that reductive cyclization of 2-(2-nitrophenyl)pyridine by trivalent phosphorus will generate pyrazolo-fused heteroaromatic pyrido[1,2-b]indazole.[52] However, for the reductive cyclization of compound **9**, a pyrazolo-fused product was not observed.

Scheme 3. Reductive cyclization of nitro-compounds.
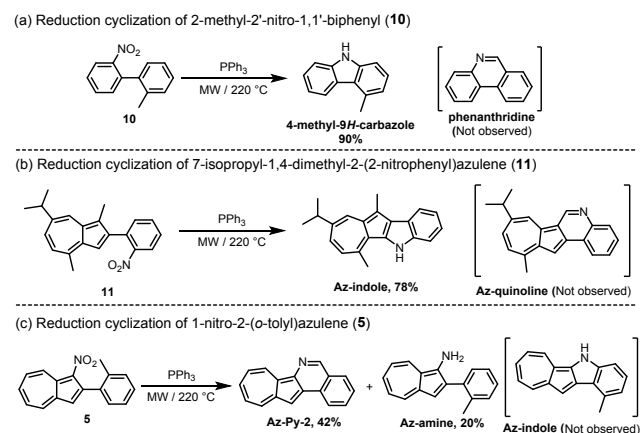
To gain insight into this reductive cyclization reaction and its selectivity, two control experiments were performed as shown in Scheme 3a and 3b. By using the same reduction conditions with 1-nitroazulene compounds, reduction of nitrophenyl compounds **10** and **11** provided pyrrole-fused 4-methyl-9*H*-carbazole and **Az-indole** in 90% and 78% yield, respectively, and pyridine-fused products phenanthridine and **Az-quinoline** were not observed. It is worth mentioning that compound **11** was chosen because it has a similar geometric disposition between the nitro and methyl group to that of compound **5**. The obvious differences are that for compound **11**, the nitro group is on the phenyl unit, and for compound **5**, the nitro group is on the azulene moiety. These results indicate that pyridine-fused heteroaromatics are generated only when the nitro group is at the 1-position of azulene and in other cases the pyrrole-fused Cadogan cyclization product is solely observed.

Scheme 4. Proposed Mechanism.
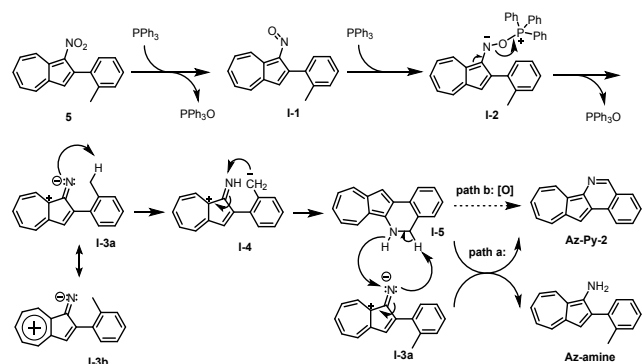
For such interesting reductive cyclization reactions, we propose the reaction mechanism shown in Scheme 4. The nitro group in compound **5** is first reduced to nitroso by one equivalence of triphenylphosphine to obtain intermediate **I-1**.[53] Then another equivalence of triphenylphosphine attacks the nitroso group in **I-1** to form intermediate **I-2**. As mentioned before, the 1-position of azulene has a strong electron-donating ability, so the elimination of one molecule of triphenylphosphine oxide by **I-2** can generate **I-3a** containing an electron-rich nitrene (Figure S3). We emphasize this character by drawing this intermediate as a zwitterion. The tropylium cation in **I-3b**, a resonance structure of **I-3a**, has 6π electrons, so this intermediate with zwitter-ionic character is promoted by aromaticity. It is the unique electronic structure of azulene, that generates the electron-rich nitrene in **I-3a** that deprotonates the benzylic hydrogen to form intermediate **I-4**. Intramolecular nucleophilic cyclization of **I-4** provides **I-5**, which can be oxidized to form the aromatic product **Az-Py-2**. As shown in Scheme 3c, about 20% yield of **Az-amine** byproduct was isolated (see SI, Figures S21 and S22 for its characterization), suggesting a possible oxidation of **I-5** by intermediate **I-3a**. The formation of the amine byproducts is the main reason for obtaining only moderate yields of azulene-pyridine fused products. It is worth mentioning that for Cadogan reaction, the nitro group on the substrate is usually

reduced to an electron-deficient nitrene, which tends to undergo an electrophilic C-H insertion reactions.[53] When the nitro group in 2-(2-nitrophenyl)pyridine is reduced to a nitrene, it attacks the pyridine nitrogen to form pyrazolo-fused product.[52] However, the nitrene obtained from the reduction of the nitro group in substrate **9** is electron-rich, and it does not react with the nitrogen on the
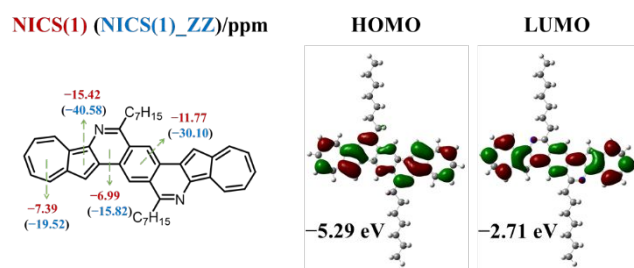
Table 1. Optical, electrochemical and DFT calculation data for Az-Py-1–Az-Py-6.

Compound	λ_{max} (nm)/($\varepsilon \times 10^{-3}$ M^{-1} cm^{-1})	E_g^{opt} (eV)[a]	Φ_F[b]	E_{onset}^{red1} (V)[c]	E_{onset}^{ox1} (V)[c]	LUMO (eV)[d]	HOMO (eV)[d]	E_g^{cv} (eV)[e]	LUMO (eV)[f]	HOMO (eV)[f]
Az-Py-1	348/86.2, 705/0.81	1.49	<0.1%	−1.68	0.25	−3.12	−5.05	1.93	−2.71	−5.29
Az-Py-2	349/61.6, 618/0.35	1.55	<0.1%	−1.70	0.35	−3.10	−5.15	2.05	−2.51	−5.45
Az-Py-3	355/60.1, 632/0.25	1.54	<0.1%	−1.67	0.31	−3.13	−5.11	1.98	−2.52	−5.40
Az-Py-4	334/63.1, 620/0.27	1.54	<0.1%	−1.71	0.27	−3.09	−5.07	1.98	−2.50	−5.41
Az-Py-5	349/47.6, 628/0.28	1.54	<0.1%	−1.70	0.28	−3.10	−5.08	1.98	−2.47	−5.38
Az-Py-6	310/45.9, 616/0.34	1.53	<0.1%	−1.57	0.41	−3.23	−5.21	1.98	−2.61	−5.52

[a] Estimated from the onset absorption. [b] Estimated in DCM by using 9,10-diphenylanthracene as reference. [c] Onset potential versus Fc/Fc+. [d] Calculated from $E_{HOMO/LUMO} = −4.80 − E_{onset}^{ox1}/ E_{onset}^{red1}$. [e] Calculated from CV. [f] Estimated from DFT calculations.

pyridine ring, so the pyrazole-fused product was not observed as previously discussed.

Figure 3. NICS values, frontier molecular orbitals and their energies of **Az-Py-1** obtained by DFT calculations.

To understand the structural and electronic properties and aromaticity of azulene- and pyridine-fused heteroaromatics, we carried out density functional theory (DFT) and nucleus-independent chemical shift (NICS) calculations on **Az-Py-1** as well as **Az-Py-2**–**Az-Py-6**. As shown in Figure S4a, all molecules exhibit a highly planar geometry, which is consistent with single crystal X-ray analysis of **Az-Py-1**. For **Az-Py-1**, the orbital coefficients of frontier molecular orbitals (FMO) are distributed over the whole backbone (Figure 3). However, it is worth noting that for the HOMO, the electron density coefficients are localized on the odd-positions and the nitrogen atoms. For the LUMO, the coefficients are large on the even-positions and the carbon atoms connected to 2-positions of azulene units. The 1-positions of azulene moieties have very minimal molecular orbital coefficients in the LUMO. **Az-Py-2**–**Az-Py-6** have similar characteristics as shown in Figure S4a. These observations are similar to those previously reported for other azulene-fused (hetero)aromatics,[45] and can be attributed to the unique molecular orbitals of azulene as mentioned before. The calculated FMO energy levels and HOMO–LUMO energy gaps of all of the **Az-Py** compounds are listed in Table 1. As expected, **Az-Py-1** with an extended π-system has a lower LUMO energy level (−2.71 eV) and higher HOMO energy level (−5.29 eV) than

Az-Py-2 (LUMO, −2.51 eV; HOMO, −5.45 eV). Adding an electron-withdrawing nitrogen atom in compound **Az-Py-6** generates a lower HOMO and LUMO energy levels (LUMO, −2.61 eV; HOMO, −5.52 eV) when compared to **Az-Py-2**. As suggested by NICS values (Figure 3 and Figure S4b), all the azulene- and pyridine-fused heteroaromatics maintain good aromaticity with highest NICS(1) value of about −7 ppm. Notably, the electron-rich five-membered rings of azulene moieties in all compounds have NICS values lower than the other rings including thiophene, which indicates that they have high aromatic character.

In order to gain insights into the origin of the absorption features of these azulene- and pyridine-fused heteroaromatics **Az-Py-1**–**Az-Py-6**, we also performed the time-dependent DFT (TD-DFT) calculations at the CAM-B3LYP /6-311g(d,p) level by using the polarizable continuum model (PCM). As shown in Figure S5a, in the low-energy region, the simulated absorption spectrum of **Az-Py-1** shows a broad and weak absorption band at 575 nm. As shown in Table S3, this low-energy absorption corresponds to the $S_0 \rightarrow S_1$ transition with a low oscillator intensity (f) of 0.024, and is attributed to a combined contribution of HOMO → LUMO (66%) and HOMO−1 → LUMO+2 (29%) transition. Compared to **Az-Py-1**, **Az-Py-2** exhibits a blue-shifted $S_0 \rightarrow S_1$ transition (λ_{cal} = 547 nm, f = 0.010) which is mainly contributed by HOMO → LUMO (96%) transitions. These characteristics are similar to those of parent azulene and azulene-based compounds, and can be attributed to the HOMO–LUMO characteristics of azulene.[2]

We investigated the optical and electrochemical properties of **Az-Py-1**–**Az-Py-6** by using UV-vis absorption spectroscopy, emission spectroscopy and cyclic voltammetry (CV) as summarized in Table 1. Figure 4 presents the absorption spectra of **Az-Py-1**–**Az-Py-6**. All of compounds show a well-resolved absorption profile with structured vibrational peaks, indicative of their rigid scaffolds. **Az-Py-2**–**Az-Py-6** have the same 18π conjugated skeleton and exhibit strong absorptions from 280 to 350

nm and moderate absorptions at 350 to 450 nm. In comparison with **Az-Py-2**, compound **Az-Py-1** with extended π-structure exhibited red-shifted absorption bands with an enhanced molar extinction coefficient ($\varepsilon_{max,Az-Py-1}$ = 86200 M^{-1}cm^{-1} versus $\varepsilon_{max,Az-Py-2}$ = 61600 M^{-1}cm^{-1}). Additionally, weak absorptions (ε= 250–810 M^{-1}cm^{-1}) can be found in the range of 550 to 800 nm for all of compounds, corresponding to their $S_0 \rightarrow S_1$ transition. The optical band gap of **Az-Py-1** calculated from the onset of the absorption is 1.49 eV, which is slightly lower than those of **Az-Py-2**–**Az-Py-6** which range from 1.53 to 1.55 eV. These results reflect the distinctive features of the azulene unit and are consistent with the aforementioned TD-DFT calculations. On the other hand, **Az-Py-1**–**Az-Py-6** are virtually nonfluorescent with fluorescence quantum yields less than 0.1%. (Table 1 and Figure S6). Nevertheless, a weak emission spectrum is observed from **Az-Py-1**–**Az-Py-6** that originates from S_2 or higher excited states and there is no detectable emission from the S_1 state (Figure S6). This phenomena are similar to what is observed for azulene,[54] and are new examples of compounds that violate Kasha's rule.[55]
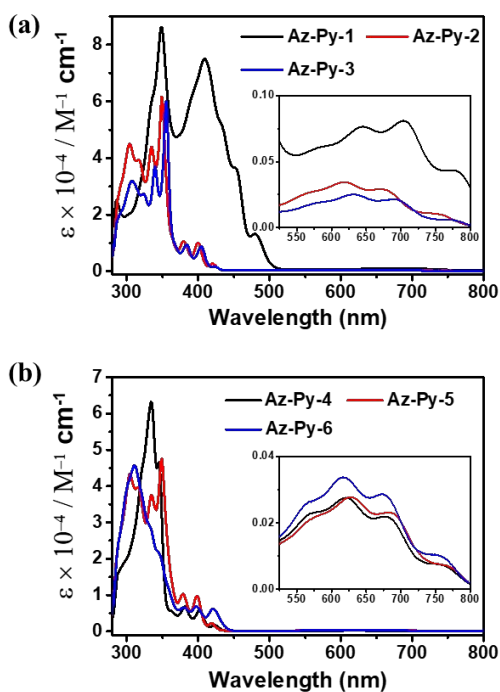
Figure 4. UV-vis spectra of **Az-Py-1**–**Az-Py-3** (a), and **Az-Py-4**–**Az-Py-6** (b) in dichloromethane solution with the magnified low-energy absorptions inserted.

As shown in Figure 5, all of the **Az-Py** products exhibit oxidation and reduction processes under the measurement conditions. **Az-Py-2**–**Az-Py-6** with the same 18π conjugated skeleton, exhibit similar CV profiles including multiple irreversible or quasi-reversible oxidation processes and one irreversible reduction wave. By contrast, **Az-Py-1**, with a more extended π-skeleton, displays multiple oxidation events containing an irreversible first oxidation wave, and two clearly visible quasi-reversible reduction peaks. The first onset oxidation potential (E_{onset}^{ox1} *vs* Fc/Fc$^+$) and first onset reduction

potential (E_{onset}^{red1} *vs* Fc/Fc$^+$) of **Az-Py-1** are 0.25 V and −1.68 V, respectively. Accordingly, the HOMO and LUMO energy levels of **Az-Py-1** evaluated by CV measurements and referenced to ferrocene (−4.8 eV versus vacuum)[56] are −5.05 eV and −3.12 eV, respectively. Compared to **Az-Py-2** ($E_{onset}^{ox1}/E_{onset}^{red1}$ = 0.35/−1.70 V), its N-doped analogue **Az-Py-6** ($E_{onset}^{ox1}/E_{onset}^{red1}$ = 0.41/−1.57 V) presents both anodically shifted oxidation and reduction potentials. Therefore, the HOMO/LUMO energy levels of **Az-Py-6** (−5.21/−3.23 eV) are lower than those of **Az-Py-2** (−5.15/−3.10 eV), which correlates well with the results by DFT calculations.
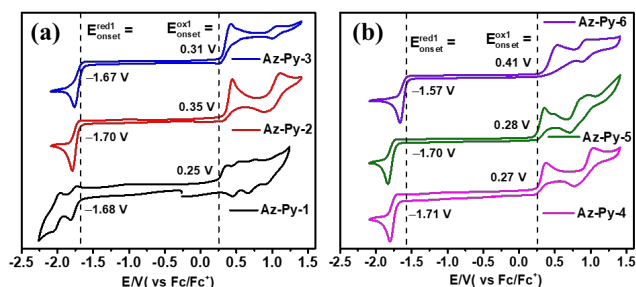
Figure 5. Cyclic voltammograms of all of the **Az-Py** compounds in dichloromethane (0.1 M Bu4$^+$NPF6$^-$ as supporting electrolyte; scan rate of 100 mV/s).

The 1- and 3-positons of azulene can be protonated by strong acid such as trifluoroacetic acid (TFA) to form a stable azulenium cation that can be neutralized by base to regenerate azulene (Scheme S1a).[57-60] On the other hand, nitrogen atom on the pyridine unit also can be protonated by acid. Therefore, we investigated the effect of protonating these azulene- and pyridine-fused heteroaromatics. As shown in Figures S7 and S8, the UV-vis absorption spectra and the colors of **Az-Py-1**–**Az-Py-6** in dichloromethane changed upon addition of 0.02% volume of TFA. The spectra and the colors of **Az-Py-1** and **Az-Py-6** are further changed when adding 2% TFA. To determine the protonating positions of these compounds, ^{1}H and ^{13}C NMR studies were performed on **Az-Py-2** and its protonated product. As shown in Figure S9, although the chemical shifts change, the number of aromatic proton and carbon peaks in protonated **Az-Py-2** remains unchanged compared to its neutral state. These results confirm that only the nitrogen atom on pyridine unit is protonated, and the azulene moiety is not. This result is further confirmed by TD-DFT calculations on protonated **Az-Py-1** and **Az-Py-2** (Figures S10 and S11). This observation can be rationalized by considering that the electron-withdrawing protonated nitrogen on the 1-position of azulene moiety deactivates the azulene core and prevents protonation.
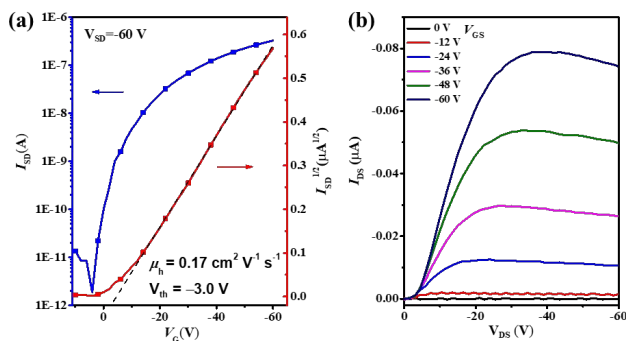
Figure 6. Transfer (a), and output (b) curves of OFET device based on crystal ribbons of **Az-Py-1**.

Judging from its conjugated π-structure, strong π-π interaction in solid state, and HOMO/LUMO energy levels, **Az-Py-1** has the proper attributes to be a high performance organic semiconducting material. As a result, we investigated the charge transport properties of **Az-Py-1** crystal ribbons *via* organic filed-effect transistor (OFET) measurements. Single crystal ribbons of **Az-Py-1** were prepared by drop-casting toluene solutions (0.5 mg/mL) onto the octadecyltrimethoxysilane (OTMS)-treated Si/SiO$_2$ substrates (Figure S12a). Au source/drain electrodes were deposited on the single crystal ribbons by the Au layer stamping technique[61] to afford a bottom-gate top-contact (BGTC) device structure (Figure S12b). More than 20 devices were fabricated and measured both in air and in N$_2$, and the performances obtained were insensitive to the atmosphere. The transfer and output curves of the OFET device are shown in Figure 6. The single crystal ribbons of **Az-Py-1** exhibit typical p-type semiconducting behavior, which correlates well with the aforementioned DFT and CV results. The average hole mobility (μ_h) extracted from the transfer curves is 0.16 cm^2 V^{-1} s^{-1} with a high current on/off ratio (I_{on}/I_{off}) of 10^5–10^6, and the highest μ_h was 0.29 m^2 V^{-1} s^{-1}, which is among the highest hole mobilities for azulene-based organic semiconductors.[4] These results demonstrate that **Az-Py-1** is a promising material for organic semiconductors.

CONCLUSION

In conclusion, an efficient synthesis of azulene-pyridine fused heteroaromatics, **Az-Py**, were synthesized by reduction of 1-nitroazulene precursors with triphenylphosphine. Studies began with the unexpected production of the extended system **Az-Py-1**, and its structure was unambiguously confirmed by single-crystal X-ray diffraction analysis. Structure property studies demonstrate that the observed reductive cyclization is promoted by electronic structure of azulene, which generates a nitrene intermediate that has a high degree of negative charge on the nitrogen. Single azulene derivatives **Az-Py-2**–**Az-Py-6** were also synthesized using this reaction, thereby establishing the utility of this method for the construction of azulene- and pyridine-fused heteroaromatics. Theoretical calculations, photophysical, electrochemical properties and protonating properties of **Az-Py-1**–**Az-Py-6** were investigated. The results revealed that these heteroaromatics display strong aromaticity with

rigid planar π-structures, and exhibit weak S$_0$ → S$_1$ transition absorptions in visible characteristic of azulene systems. Single crystal ribbons of **Az-Py-1** exhibit p-type semiconducting behavior with hole mobilities of up to 0.29 m^2 V^{-1} s^{-1}. We conclude that these methods afford access to new azulene- and pyridine-fused heteroaromatics with promising characteristics as organic electronic materials.

ASSOCIATED CONTENT

Detailed methods, synthesis, characterization data, crystal data of **Az-Py-1** and additional figures. This material is available free of charge via the Internet at http://pubs.acs.org.

AUTHOR INFORMATION

Corresponding Author

* tswager@mit.edu
* gaoxk@mail.sioc.ac.cn

Author Contributions

The manuscript was written through contributions of all authors. / All authors have given approval to the final version of the manuscript.

Notes

The authors declare no competing financial interest.
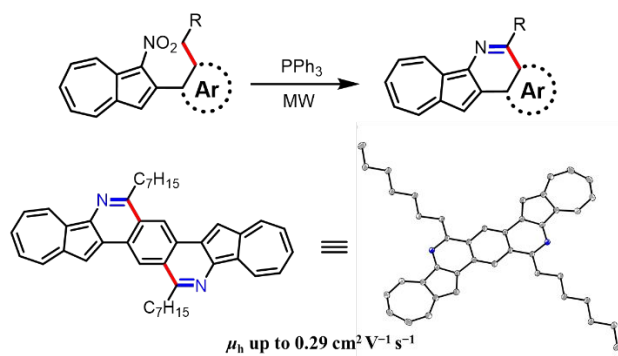
ACKNOWLEDGMENT

REFERENCES

(1).   Anderson Jr, A. G.; Steckler, B. M., Azulene. VIII. A Study of the Visible Absorption Spectra and Dipole Moments of Some 1- and 1, 3-Substituted Azulenes. *J. Am. Chem. Soc.* **1959,** *81*, 4941-4946.

(2).   Michl, J.; Thulstrup, E. W. J. T., Why is azulene blue and anthracene white? A simple MO picture. *Tetrahedron* **1976,** *32*, 205-209.

(3).   Ito, S.; Morita, N., Creation of Stabilized Electrochromic Materials by Taking Advantage of Azulene Skeletons. *Eur. J. Org. Chem.* **2009,** *2009*, 4567-4579.

(4).   Xin, H.; Gao, X. J. C., Application of azulene in constructing organic optoelectronic materials: new tricks for an old dog. *ChemPlusChem* **2017,** *82*, 945-956.

(5).   Wang, X.; Ng, J. K.-P.; Jia, P.; Lin, T.; Cho, C. M.; Xu, J.; Lu, X.; He, C., Synthesis, Electronic, and Emission Spectroscopy, and Electrochromic Characterization of Azulene–Fluorene Conjugated Oligomers and Polymers. *Macromolecules* **2009,** *42*, 5534-5544.

(6).   Amir, E.; Amir, R. J.; Campos, L. M.; Hawker, C. J., Stimuli-responsive azulene-based conjugated oligomers with polyaniline-like properties. *J. Am. Chem. Soc.* **2011,** *133*, 10046-10049.

(7).   Usui, K.; Tanoue, K.; Yamamoto, K.; Shimizu, T.; Suemune, H., Synthesis of substituted azulenes via Pt(II)-catalyzed ring-expanding cycloisomerization. *Org. Lett.* **2014,** *16*, 4662-4665.

(8).   Cowper, P.; Jin, Y.; Turton, M. D.; Kociok-Kohn, G.; Lewis, S. E., Azulenesulfonium Salts: Accessible, Stable, and Versatile Reagents for Cross-Coupling. *Angew. Chem. Int. Ed.* **2016,** *55*, 2564-2568.

(9).   Lash, T. D., Out of the Blue! Azuliporphyrins and Related Carbaporphyrinoid Systems. *Acc. Chem. Res.* **2016,** *49*, 471-482.

(10). Szekely, A.; Peter, A.; Aradi, K.; Tolnai, G. L.; Novak, Z., Gold-Catalyzed Direct Alkynylation of Azulenes. *Org. Lett.* **2017,** *19*, 954-957.

(11). Mishra, S.; Lohr, T. G.; Pignedoli, C. A.; Liu, J.; Berger, R.; Urgel, J. I.; Mullen, K.; Feng, X.; Ruffieux, P.; Fasel, R., Tailoring Bond Topologies in Open-Shell Graphene Nanostructures. *ACS Nano* **2018,** *12*, 11917-11927.

(12). Narita, M.; Murafuji, T.; Yamashita, S.; Fujinaga, M.; Hiyama, K.; Oka, Y.; Tani, F.; Kamijo, S.; Ishiguro, K., Synthesis of 2-Iodoazulenes by the Iododeboronation of Azulen-2-ylboronic Acid Pinacol Esters with Copper(I) Iodide. *J. Org. Chem.* **2018,** *83*, 1298-1303.

(13). Konishi, A.; Morinaga, A.; Yasuda, M., Construction of Polycyclic pi-Conjugated Systems Incorporating an Azulene Unit Following the Oxidation of 1,8-Diphenyl-9,10-bis(phenylethynyl)phenanthrene. *Chem. Eur. J.* **2018,** *24*, 8548-8552.

(14). Zhou, Y.; Baryshnikov, G.; Li, X.; Zhu, M.; Ågren, H.; Zhu, L., Anti-Kasha's Rule Emissive Switching Induced by Intermolecular H-Bonding. *Chem. Mater.* **2018,** *30*, 8008-8016.

(15). Chaolumen; Ito, H.; Itami, K., An axially chiral 1,1'-biazulene and its pi-extended derivative: synthesis, structures and properties. *Chem. Commun.* **2019,** *55*, 9606-9609.

(16). Amir, E.; Murai, M.; Amir, R. J.; Cowart, J. S.; Chabinyc, M. L.; Hawker, C. J., Conjugated oligomers incorporating azulene building blocks – seven- vs. five-membered ring connectivity. *Chem. Sci.* **2014,** *5*, 4483-4489.

(17). Scheetz, K. J.; Spaeth, A. D.; Vorushilov, A. S.; Powell, D. R.; Day, V. W.; Barybin, M. V., The 2,6-dimercaptoazulene motif: efficient synthesis and completely regioselective metallation of its 6-mercapto terminus. *Chem. Sci.* **2013,** *4*, 4267–4272.

(18). Shoji, T.; Sugiyama, S.; Kobayashi, Y.; Yamazaki, A.; Ariga, Y.; Katoh, R.; Wakui, H.; Yasunami, M.; Ito, S., Direct synthesis of 2-arylazulenes by [8+2] cycloaddition of 2H-cyclohepta[b]furan-2-ones with silyl enol ethers. *Chem. Commun.* **2020,** *56*, 1485-1488.

(19). Dyker, G.; Borowski, S.; Heiermann, J.; Körning, J.; Opwis, K.; Henkel, G.; Köckerling, M., First intermolecular palladium catalyzed arylation of an unfunctionalized aromatic hydrocarbon. *J. Organomet. Chem.* **2000,** *606*, 108-111.

(20). Smits, E. C. P.; Setayesh, S.; Anthopoulos, T. D.; Buechel, M.; Nijssen, W.; Coehoorn, R.; Blom, P. W. M.; de Boer, B.; de Leeuw, D. M., Near-Infrared Light-Emitting Ambipolar Organic Field-Effect Transistors. *Adv. Mater.* **2007,** *19*, 734-738.

(21). Yamaguchi, Y.; Ogawa, K.; Nakayama, K.; Ohba, Y.; Katagiri, H., Terazulene: a high-performance n-type organic field-effect transistor based on molecular orbital distribution control. *J. Am. Chem. Soc.* **2013,** *135*, 19095-19098.

(22). Yamaguchi, Y.; Takubo, M.; Ogawa, K.; Nakayama, K.-i.; Koganezawa, T.; Katagiri, H., Terazulene isomers: polarity change of OFETs through molecular orbital distribution contrast. *J. Am. Chem. Soc.* **2016,** *138*, 11335-11343.

(23). Xin, H.; Ge, C.; Yang, X.; Gao, H.; Yang, X.; Gao, X., Biazulene diimides: a new building block for organic electronic materials. *Chem. Sci.* **2016,** *7*, 6701-6705.

(24). Yao, J.; Cai, Z.; Liu, Z.; Yu, C.; Luo, H.; Yang, Y.; Yang, S.; Zhang, G.; Zhang, D., Tuning the Semiconducting Behaviors of New Alternating Dithienyldiketopyrrolopyrrole–Azulene Conjugated Polymers by Varying the Linking Positions of Azulene. *Macromolecules* **2015,** *48*, 2039-2047.

(25). Xin, H.; Ge, C.; Jiao, X.; Yang, X.; Rundel, K.; McNeill, C. R.; Gao, X., Incorporation of 2,6-Connected Azulene Units into the Backbone of Conjugated Polymers: Towards High-Performance Organic Optoelectronic Materials. *Angew. Chem. Int. Ed.* **2018,** *57*, 1322-1326.

(26). Xin, H.; Li, J.; Ge, C.; Yang, X.; Xue, T.; Gao, X., 6,6′-Diaryl-substituted biazulene diimides for solution-processable high-performance n-type organic semiconductors. *Mater. Chem. Front.* **2018,** *2*, 975-985.

(27). Shibuya, Y.; Aonuma, K.; Kimura, T.; Kaneko, T.; Fujiwara, W.; Yamaguchi, Y.; Kumaki, D.; Tokito, S.; Katagiri, H., Linear Biazulene Isomers: Effects of Molecular and Packing Structure on Optoelectronic and Charge-Transport Properties. *J. Phys. Chem. C* **2020,** *124*, 4738-4746.

(28). Puodziukynaite, E.; Wang, H. W.; Lawrence, J.; Wise, A. J.; Russell, T. P.; Barnes, M. D.; Emrick, T., Azulene methacrylate polymers: synthesis, electronic properties, and solar cell fabrication. *J. Am. Chem. Soc.* **2014,** *136*, 11043-11049.

(29). Nishimura, H.; Ishida, N.; Shimazaki, A.; Wakamiya, A.; Saeki, A.; Scott, L. T.; Murata, Y., Hole-Transporting Materials with a Two-Dimensionally Expanded pi-System around an Azulene Core for Efficient Perovskite Solar Cells. *J. Am. Chem. Soc.* **2015,** *137*, 15656-15659.

(30). Bendikov, M.; Wudl, F.; Perepichka, D. F., Tetrathiafulvalenes, Oligoacenenes, and Their Buckminsterfullerene Derivatives: The Brick and Mortar of Organic Electronics. *Chem. Rev.* **2004,** *104*, 4891-4946.

(31). Anthony, J. E., Functionalized Acenes and Heteroacenes for Organic Electronics. *Chem. Rev.* **2006,** *106*, 5028-5048.

(32). Wu, J.; Pisula, W.; Müllen, K., Graphenes as Potential Material for Electronics. *Chem. Rev.* **2007,** *107*, 718-747.

(33). Maliakal, A.; Raghavachari, K.; Katz, H.; Chandross, E.; Siegrist, T., Photochemical Stability of Pentacene and a Substituted Pentacene in Solution and in Thin Films. *Chem. Mater.* **2004,** *16*, 4980-4986.

(34). Payne, M. M.; Parkin, S. R.; Anthony, J. E., Functionalized Higher Acenes: Hexacene and Heptacene. *J. Am. Chem. Soc.* **2005,** *127*, 8028-8029.

(35). Kaur, I.; Jia, W.; Kopreski, R. P.; Selvarasah, S.; Dokmeci, M. R.; Pramanik, C.; McGruer, N. E.; Miller, G. P., Substituent Effects in Pentacenes: Gaining Control over HOMO–LUMO Gaps and Photooxidative Resistances. *J. Am. Chem. Soc.* **2008,** *130*, 16274-16286.

(36). Stepien, M.; Gonka, E.; Zyla, M.; Sprutta, N., Heterocyclic Nanographenes and Other Polycyclic Heteroaromatic Compounds: Synthetic Routes, Properties, and Applications. *Chem. Rev.* **2017,** *117*, 3479-3716.

(37). Koide, T.; Takesue, M.; Murafuji, T.; Satomi, K.; Suzuki, Y.; Kawamata, J.; Terai, K.; Suzuki, M.; Yamada, H.; Shiota, Y.; Yoshizawa, K.; Tani, F., An Azulene-Fused Tetracene Diimide with a Small HOMO-LUMO Gap. *ChemPlusChem* **2017,** *82*, 1010-1014.

(38). Murai, M.; Iba, S.; Ota, H.; Takai, K., Azulene-Fused Linear Polycyclic Aromatic Hydrocarbons with Small Bandgap, High Stability, and Reversible Stimuli Responsiveness. *Org. Lett.* **2017,** *19*, 5585-5588.

(39). Jiang, Q.; Tao, T.; Phan, H.; Han, Y.; Gopalakrishna, T. Y.; Herng, T. S.; Li, G.; Yuan, L.; Ding, J.; Chi, C., Diazuleno-s-indacene Diradicaloids: Syntheses, Properties, and Local (anti)Aromaticity Shift from Neutral to Dicationic State. *Angew. Chem. Int. Ed.* **2018,** *57*, 16737-16741.

(40). Yamamoto, K.; Ie, Y.; Tohnai, N.; Kakiuchi, F.; Aso, Y., Antiaromatic character of cycloheptatriene-bis-annelated indenofluorene framework mainly originated from heptafulvene segment. *Sci. Rep.* **2018,** *8*, 17663.

(41). Yang, X.; Rominger, F.; Mastalerz, M., Contorted Polycyclic Aromatic Hydrocarbons with Two Embedded Azulene Units. *Angew. Chem. Int. Ed.* **2019,** *58*, 17577-17582.

(42). Sasaki, Y.; Takase, M.; Okujima, T.; Mori, S.; Uno, H., Synthesis and Redox Properties of Pyrrole- and Azulene-Fused Azacoronene. *Org. Lett.* **2019,** *21*, 1900-1903.

(43). Konishi, A.; Horii, K.; Shiomi, D.; Sato, K.; Takui, T.; Yasuda, M., Open-Shell and Antiaromatic Character Induced by the Highly Symmetric Geometry of the Planar Heptalene Structure: Synthesis and Characterization of a Nonalternant Isomer of Bisanthene. *J. Am. Chem. Soc.* **2019,** *141*, 10165-10170.

(44). Liu, J.; Mishra, S.; Pignedoli, C. A.; Passerone, D.; Urgel, J. I.; Fabrizio, A.; Lohr, T. G.; Ma, J.; Komber, H.; Baumgarten, M.; Corminboeuf, C.; Berger, R.; Ruffieux, P.; Mullen, K.; Fasel, R.; Feng,

X., Open-Shell Nonbenzenoid Nanographenes Containing Two Pairs of Pentagonal and Heptagonal Rings. *J. Am. Chem. Soc.* **2019,** *141*, 12011-12020.

(45). Xin, H.; Li, J.; Yang, X.; Gao, X., Azulene-Based BN-Heteroaromatics. *J. Org. Chem.* **2020,** *85*, 70-78.

(46). Zhang, X.-S.; Huang, Y.-Y.; Zhang, J.; Meng, W.; Peng, Q.; Kong, R.; Xiao, Z.; Liu, J.; Huang, M.; Yi, Y.; Chen, L.; Fan, Q.; Lin, G.; Liu, Z.; Zhang, G.; Jiang, L.; Zhang, D., Dicyclohepta [ijkl, uvwx] rubicene with Two Pentagons and Two Heptagons as a New Stable and Planar Non‐benzenoid Nanographene. *Angew. Chem. Int. Ed.* **2020,** *59*, 3529–3533.

(47). Ma, J.; Fu, Y.; Dmitrieva, E.; Liu, F.; Komber, H.; Hennersdorf, F.; Popov, A. A.; Weigand, J. J.; Liu, J.; Feng, X., Helical Nanographenes Containing an Azulene Unit: Synthesis, Crystal Structures, and Properties. *Angew. Chem. Int. Ed.* **2020,** *59*, 5637-5642.

(48). Han, Y.; Xue, Z.; Li, G.; Gu, Y.; Ni, Y.; Dong, S.; Chi, C., Formation of Azulene‐Embedded Nanographene: Naphthalene to Azulene Rearrangement During the Scholl Reaction. *Angew. Chem. Int. Ed.* **2020,** *59*, 9026-9031.

(49). McDonald, R. N.; Richmond, J. M., Nonbenzenoid aromatic systems. XI. Synthesis and buffered acetolysis of 2-(2-azulyl)ethyl tosylate and nosylate. *J. Org. Chem.* **1975,** *40*, 1689-1694.

(50). Chen, H.-Y.; Chen, C.-T.; Chen, C.-T., Synthesis and Characterization of a New Series of Blue Fluorescent 2,6-Linked 9,10-Diphenylanthrylenephenylene Copolymers and Their Application for Polymer Light-Emitting Diodes. *Macromolecules* **2010,** *43*, 3613-3623.

(51). Allen, F. H.; Kennard, O.; Watson, D. G.; Brammer, L.; Orpen, A. G.; Taylor, R., Tables of bond lengths determined by X-ray and neutron diffraction. Part 1. Bond lengths in organic compounds. *J. Chem. Soc., Perkin Trans. 2* **1987**, S1-S19.

(52). Cadogan, J. I. G.; Cameron-Wood, M.; Mackie, R. K.; Searle, R. J. G., 896. The reactivity of organophosphorus compounds. Part XIX. Reduction of nitro-compounds by triethyl phosphite: a convenient new route to carbazoles, indoles, indazoles, triazoles, and related compounds. *J. Chem. Soc.* **1965**, 4831-4837.

(53). Kaur, M.; Kumar, R., C‐N and N‐N bond formation via Reductive Cyclization: Progress in Cadogan /Cadogan‐Sundberg Reaction. *ChemistrySelect* **2018,** *3*, 5330-5340.

(54). Sidman, J. W.; McClure, D. S., Electronic and Vibrational States of Azulene. *J. Chem. Phys.* **1956,** *24*, 757-763.

(55). Kasha, M., Characterization of electronic transitions in complex molecules. *Discuss. Faraday Soc.* **1950,** *9*, 14-19.

(56). Pommerehne, J.; Vestweber, H.; Guss, W.; Mahrt, R. F.; Bässler, H.; Porsch, M.; Daub, J., Efficient two layer leds on a polymer blend basis. *Adv. Mater.* **1995,** *7*, 551-554.

(57). Kihara, N.; Nakayama, H.; Fukutomi, T., True Polyazulene: Soluble Precursor of So-Called "Polyazulene". *Macromolecules* **1997,** *30*, 6385-6387.

(58). Murai, M.; Amir, E.; Amir, R. J.; Hawker, C. J., Azulene-based conjugated polymers: unique seven-membered ring connectivity leading to stimuli-responsiveness. *Chem. Sci.* **2012,** *3*, 2721-2725.

(59). Murai, M.; Ku, S.-Y.; Treat, N. D.; Robb, M. J.; Chabinyc, M. L.; Hawker, C. J., Modulating structure and properties in organic chromophores: influence of azulene as a building block. *Chem. Sci.* **2014,** *5*, 3753-3760.

(60). Venkatesan, M. K. B., Syntheses and Tunable Emission Properties of 2-Alkynyl Azulenes. *Org,Lett.* **2012,** *14*, 1580–1583.

(61). Tang, Q.; Jiang, L.; Tong, Y.; Li, H.; Liu, Y.; Wang, Z.; Hu, W.; Liu, Y.; Zhu, D., Micrometer- and Nanometer-Sized Organic Single-Crystalline Transistors. *Adv. Mater.* **2008,** *20*, 2947-2951.

Insert Table of Contents artwork here

μ_h up to 0.29 cm^2 V^{-1} s^{-1}